

SUPPRESSING CSR MICROBUNCHING IN RECIRCULATION ARCS*

Cheng-Ying Tsai[†]

SLAC National Accelerator Laboratory, Menlo Park, California, USA

Abstract

In this paper we give an overview of existing mitigation schemes of coherent synchrotron radiation (CSR) effects, including compensation of CSR-induced emittance growth and suppression of CSR microbunching instabilities in multi-bend beam transport or recirculation arcs. We provide a set of sufficient conditions for suppression of CSR-induced microbunching instability along transport or recirculation arcs. The example lattices include two comparative 1.3 GeV high-energy recirculation arcs.

Our studies show that lattices satisfying the proposed conditions indeed have microbunching amplification gain suppressed. Beam current dependencies of maximal CSR microbunching gains are also demonstrated, which should help outline a beamline design for different scales of nominal currents. We expect this analysis can shed light on future lattice design approach which aims to control the CSR-induced microbunching.

INTRODUCTION

Coherent synchrotron radiation (CSR) has been recognized as one of the most challenging issues for high-brightness beam transport system and recirculation machine designs, in which the beam phase-space quality is always aimed to preserve as well as possible before the beam fulfills its scientific mission or is transported to a subsequent beamline complex. CSR can be generated from electron coherent radiation emission inside a bend at a wavelength range comparable to the bunch length scale or to the order of the density fluctuations atop.

The radiation reaction can have effects on both transverse and longitudinal planes. In the transverse plane, because of the dispersive nature of a bending system, the energy change due to CSR can be correlated to the transverse coordinates (x or x') through the dispersion functions (R_{16} or R_{26}). Since the energy change varies for different bunch slices, such energy variation within a whole beam can potentially dilute the projected transverse emittance. In the longitudinal plane, initial small density modulations can be converted into energy modulations due to the tail-head collective interaction. Then the energy modulations can be transformed back to density counterparts downstream in dispersive regions via momentum compaction (R_{56}).

The density-energy conversion, if forming a positive feedback in a multibend system, can result in the enhancement

of modulation amplitudes. This has been known as the CSR-induced microbunching instability (MBI) [1–3].

OVERVIEW OF EXISTING MITIGATION SCHEMES

Transverse Domain

Various mitigation schemes have been proposed to minimize or cancel the CSR-induced emittance growth. For example, Hajima [4] used the beam envelope matching method by characterizing the transverse phase-space ellipse tilt due to CSR. This method concludes that with proper arrangement of lattice optics in a unit cell along the major axis of the transverse beam phase space ellipse, the beam emittance growth due to steady-state CSR can be minimized. Figure 1 illustrates the concept. Jing *et al.* [5] studied a similar concept for ERL-based FEL in eRHIC. Douglas [6–9] and Di Mitri *et al.* [10] employed the cell-to-cell phase matching to compensate or cancel the CSR kicks.

The strategy is schematically illustrated in Fig. 2. With dedicated beamline design, this approach can achieve the cancellation of CSR-induced emittance growth. Jiao *et al.* [11] extended the above two methods to give generic conditions for suppression of the CSR-induced emittance growth in a two-dipole achromat unit. Di Mitri and Cornacchia [12] also extended their previous analysis [10] to the case of compressor arcs. Other specialized idea to manipulate the beam conditions can be found in Ref. [14].

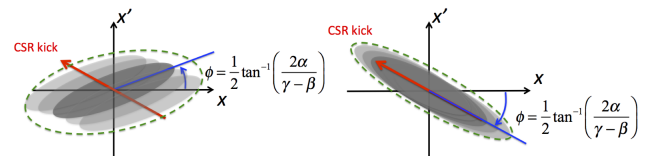


Figure 1: Illustration of CSR-induced transverse phase space dilution. In the left figure the emittance growth due to CSR-kick is larger than the right figure because of the difference of phase space orientation (or tilt angle ϕ).

The general discussion of transverse emittance preservation due to CSR was made by Emma, Brinkmann [15] and recently elaborated by Venturini [16,17]. The condition of minimizing (or vanishing) the beam emittance can be formulated to be $\int_{s_i}^{s_f} g(s)R_{16}^{s \rightarrow s_f}(s)ds = 0$ and $\int_{s_i}^{s_f} g(s)R_{26}^{s \rightarrow s_f}(s)ds = 0$, where the definitions of s, s_i, s_f are shown in Fig. 3 and $g(s) = (\kappa/\rho(s))^{2/3}$ inside a dipole and 0 elsewhere (κ is a constant).

Assuming the same dipole radius in a specific unit cell, the condition can be re-written as $R_{16}^{s_1 \rightarrow s_f} = -R_{16}^{s_2 \rightarrow s_f}$ and

* This work was supported by Jefferson Science Associates, LLC under U.S. DOE Contract No. DE-AC05-06OR23177 and is supported by the US Department of Energy (DOE) under contract DE-AC02-76SF00515 and the US DOE Office of Science Early Career Research Program grant FWP-2013-SLAC-100164 at the preparation of the manuscript.

[†] jcytsai@slac.stanford.edu

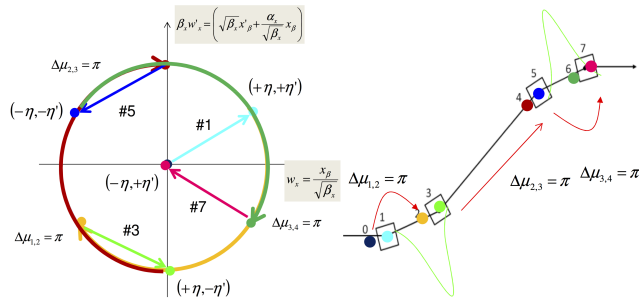


Figure 2: Illustration of cell-to-cell phase matching to cancel the CSR kick (left) and a four-dipole transport line (right). η and η' are dispersion and its derivative due to CSR kick. The CSR kick causes a shift (of reference particle) in the (normalized) transverse phase space. The design optics gives a betatron phase advance of π in the bending plane between two consecutive dipoles. It corresponds to a clockwise π rotation. Picture from Ref. [13].

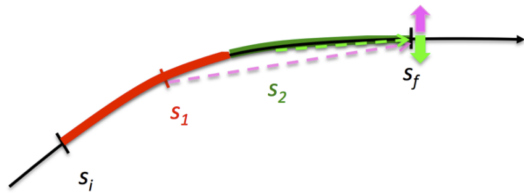


Figure 3: Conceptual illustration of CSR-induced energy kicks generated from s_1 and s_2 and eventually cancelled at s_f . Here $s_1 \in S_1$, $s_2 \in S_2$, $s_1 < s_2$, and $S_1 \cup S_2 = [s_i, s_f]$.

$R_{26}^{s_1 \rightarrow s_f} = -R_{26}^{s_2 \rightarrow s_f}$, where s_1 and s_2 are assigned as shown in Fig. 3. The analysis concludes that the above conditions lead to the two sub-cases: $\mathbf{R}_{2 \times 2}^{s_1 \rightarrow s_2} = -\mathbf{I}$ or $\mu_{1 \rightarrow 2} = \pi$ or $\mathbf{R}_{2 \times 2}^{s_1 \rightarrow s_2} = \mathbf{I}$ or $\mu_{1 \rightarrow 2} = 2\pi$ between the dipoles in a cell, where μ is the betatron phase advance and $\mathbf{R}_{2 \times 2}$ is the standard two-by-two (x, x') transfer matrix. The two explicit conditions may explain why many low-emittance beamline lattices employ π or 2π phase difference between neighboring cell units or superperiods. Below we will see that this condition becomes more stringent for CSR microbunching suppression.

Longitudinal Domain

It is typical to quantify MBI by the amplification gain $G(k)$, defined as $b(k; s_f) = G(k) \cdot b(k; s_0)$, where b is the bunching factor. The mitigation of MBI can be undertaken from either keeping $b(k; s_0)$ small or the suppression of amplification mechanism [i.e., keeping $\max G(k)$ small]. The former depends on the manipulation of bunch current distribution at some particular locations, e.g., mostly at the upstream electron gun system. As for the latter, it can usually be related to dedicated beamline designs and is the primary interest of this paper.

Without going into details of the microbunching analysis, here we only summarize the results. The resultant equation that governs the evolution of the bunching factor along a

beamline can be written in the following integral equation

$$b(k; s) = b_0(k; s) + i \int_0^s ds' \Lambda \mathcal{K}(s, s') b(k; s'), \quad (1)$$

where s' denotes the location where CSR emission may occur and s denotes the location where the beam bunch receives the CSR energy kick. The bunching factors $b(k; s)$ and $b_0(k; s)$ are defined as the Fourier transformation of the longitudinal z coordinate for perturbed and unperturbed phase space density modulation, respectively. The coefficient Λ characterizes the beam current and energy dependence $\Lambda = I_b / \gamma I_A$, where γ is the relativistic factor, I_b is the instantaneous beam current (depends on path length when bunch length varies), and I_A is the Alfvén current. The kernel function in Eq. (1) is particularly expressed as

$$\mathcal{K}(s, s') = k(s) R_{56}^{s' \rightarrow s} Z_{CSR}^{ss}(k; s') \{L.D.; s, s'\} \quad (2)$$

where, of our primary interest, only the one-dimensional steady-state free-space CSR impedance (per unit length) is considered; that is, $Z_{CSR}^{ss}(k(s); s) = (1.63 + 0.94i)(k(s)^{1/3} / |\rho(s)|^{2/3})$ [18], where $k = 2\pi/\lambda$ is the spatial wavenumber (with λ the modulation wavelength), ρ is the bending radius of a dipole, the transport matrix elements $R_{56}^{s' \rightarrow s} = [\mathbf{R}^{s' \rightarrow s}]_{56} = [\mathbf{R}^{0 \rightarrow s} (\mathbf{R}^{0 \rightarrow s'})^{-1}]_{56}$ and the Landau damping (phase smearing) term $\{L.D.; s, s'\} =$

$$\exp \left\{ \begin{aligned} & -\frac{k_0^2 \epsilon_{x0} \beta_{x0}}{2} \left[R_{51}(s, s') - \frac{\alpha_{x0}}{\beta_{x0}} R_{52}(s, s') \right]^2 \\ & -\frac{k_0^2 \epsilon_{x0}}{2} R_{52}^2(s, s') - \frac{k_0^2 \sigma_{\delta 0}^2}{2} R_{56}^2(s, s') \end{aligned} \right\}, \quad (3)$$

with $k_0 = k(s=0)$. ϵ_{x0} is the horizontal geometric emittance, α_{x0} and β_{x0} are the initial Twiss parameters, and $\sigma_{\delta 0}$ is the rms uncorrelated relative energy spread assuming Gaussian energy distribution. $R_{5i}(s, s') = C(s) R_{5i}(s) - C(s') R_{5i}(s')$, where $i = 1, 2, 6$, and $C(s) = [1 - h R_{56}(s)]^{-1}$ is the bunch compression factor, and h is the initial chirp of the beam (assuming $z > 0$ for the bunch head). Here we note that the above expressions are applicable to combined-function dipoles.

The strategy of the beamline designs for mitigation of CSR microbunching becomes clear now and can be further categorized into two types:

- (i) make the relative momentum compaction function $R_{56}^{s' \rightarrow s}$ as small as possible throughout the beamline;
- (ii) enhance the Landau damping through the exponent term of $\{L.D.; s, s'\}$.

Regarding (ii), laser heating [19, 20] has been commonly employed in linac-based FEL facilities to effectively suppress MBI. The basic idea is to use a laser beam to interact with electrons in a short undulator to induce an additional energy spread in order to enhance the Landau damping (or

Any distribution of this work must maintain attribution to the author(s), title of the work, publisher, and DOI. Content from this work may be used under the CC BY 3.0 licence (© 2018).

phase smearing). In addition to the laser heating technique, the electron-magnetic-phase mixing was also proposed [21]. The magnetically mixing chicane is utilized to smoothen the bunch current and energy distribution by forcing the electrons smear (or, slip) in the longitudinal phase space. It has been experimentally demonstrated that MBI using this technique can be reduced by an order of magnitude [21].

Other specialized beamline designs to mitigate the MBI have also been proposed. For example, by adding a set of transverse deflecting RF cavities upstream and downstream of a bunch compressor can increase an additional Landau damping and thus effectively suppress the MBI [22]. The additional energy spread is introduced in the first RF cavity, which is used to suppress the microbunching instability, and then the induced energy spread is eliminated in the second RF cavity. In Ref. [23], Qiang *et al.* proposed an inexpensive scheme to suppress MBI in a linac-based x-ray FEL light source by inserting a pair of bending magnets in the accelerator transport system. This setup can induce the longitudinal mixing associated with the transverse spread of the beam, i.e., increasing the Landau damping term via Eq. (3).

Pursuing the other path, we have recently demonstrated a set of recirculation arc lattices specifically for control of CSR and microbunching effects during transport of high brightness electron beams [7, 9]. The basic idea behind the design strategy is based on (i), to make the recirculation arc achromatic and locally isochronous. The local isochronicity insures that the bunch length be kept the same at phase homologous CSR emission sites. The local isochronicity can result in small relative momentum compaction function throughout the beamline.

OPTICS CONDITIONS FOR CSR MICROBUNCHING SUPPRESSION

Let us introduce a parameter, which we will use to characterize the CSR effect in a beamline lattice [25]

$$\xi = \left| \max \left\{ R_{56}^{s' \rightarrow s} \right\} \frac{k^{1/3}}{\rho^{2/3}} \Delta L \right|, \quad (4)$$

where ΔL is the *effective* distance of CSR interaction. It is evaluated to be the length between repetitive patterns of largest $|R_{56}^{s' \rightarrow s}|$ in a beamline design, because they usually characterize the most contributed CSR microbunching gain development [24]. In case there is not a clear repetitive structure in $|R_{56}^{s' \rightarrow s}|$, usually in arc compressors, the effective distance can be estimated as the width of the largest $|R_{56}^{s' \rightarrow s}|$ block.

It has been found that ξ , together with the concept of multistage CSR amplification [24], can be used to quantify the lattice impact of CSR microbunching. Note that ξ is independent of beam properties. The dependence of beam parameters goes in Λ and Landau damping term through Eq. (3). In the subsequent discussion of this section regarding conditions of suppression of CSR-induced microbunching gain, we have excluded the effect of Landau damping; we only aim to reach small $|R_{56}^{s' \rightarrow s}|$ of beamline optics, thus

small ξ , in order to eventually have small kernel function \mathcal{K} . However, when demonstrating example lattices in the next section, we include all relevant beam dynamics in the calculation of CSR microbunching for thorough consideration.

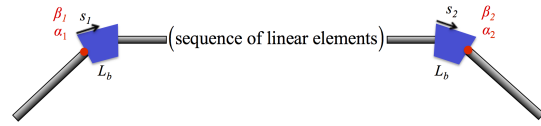


Figure 4: Illustration of a two-dipole system. The in-between section can be a general transport section. (see context for definition of notations).

Below we consider a generic transport line as shown in Fig. 4. We want to formulate in terms of typical Twiss parameters the relative momentum compaction function $R_{56}^{s_1 \rightarrow s_2}$, where inside the two dipoles, s_1 and s_2 are measured from entrances of their corresponding dipoles. We then assume the bend-plane of the beamline lattice lies in (x, z) . The four-by-four linear transport matrix from the CSR emission site (s_1) to receiving site (s_2) can be obtained by $\mathbf{R}^{\text{total}} = \mathbf{R}^{s_2 \rightarrow L_b} \mathbf{R}^{s_1 \rightarrow s_2} \mathbf{R}^{L_b \rightarrow s_1}$, i.e.,

$$\mathbf{R}^{s_1 \rightarrow s_2} = \mathbf{R}^{\text{dipole}} \left(\theta = -\frac{L_b - s_2}{\rho_2} \right) \mathbf{R}^{\text{total}} \mathbf{R}^{\text{dipole}} \left(\theta = \frac{-s_1}{\rho_1} \right), \quad (5)$$

where the transport matrix for a sector dipole can be easily expressed and that for the total transport section can be generally parameterized by Twiss parameters with $\alpha_1, \alpha_2, \beta_1$, and β_2 are assigned in Fig. 4. The relative momentum compaction function $R_{56}^{s_1 \rightarrow s_2}$ can then be analytically obtained [25]. By examining the parametric dependencies of $R_{56}^{s_1 \rightarrow s_2}$ on Twiss parameters α, β and the betatron phase difference ψ_{21} , we conclude that, to reach small $R_{56}^{s_1 \rightarrow s_2}$, small β function (within dipoles) is preferred while the choice of α function (within dipoles) does not affect too much, but should avoid smallness, the resultant $R_{56}^{s_1 \rightarrow s_2}$. Furthermore, it is found that $\psi_{21} \approx \pi$ (or its integer multiples) can lead to minimal $R_{56}^{s_1 \rightarrow s_2}$. These optics conditions are found to be valid in a broad range of practical beam and lattice parameters.

The small $|R_{56}^{s_1 \rightarrow s_2}|$ (and hence small \mathcal{K}) will eventually bring about effective CSR microbunching suppression. Here we note that, although there is not a stability margin for $|R_{56}^{s_1 \rightarrow s_2}|$ (or \mathcal{K}) in an absolute sense to have effective CSR gain suppression, since the collective interaction is intensity dependent (through Λ), our proposed optics conditions shall minimize the CSR-induced microbunching gain for any given beam current level. We also emphasize that these conditions are sufficient; other schemes of making small \mathcal{K} are not excluded, e.g., Refs. [21–23] through enhancing Landau damping.

RECIRCULATION ARC EXAMPLES

To examine the proposed optics conditions for suppression of CSR microbunching, in this section we illustrate the two

comparative high-energy recirculation arcs. For more complete analysis we refer the interest reader to the published paper [25] for low-energy (~ 100 MeV) recirculation arcs and the mid-energy (~ 0.75 GeV) arc compressor designs.

High-Energy Recirculation Arcs

The first set of comparative examples involves two 1.3-GeV high-energy recirculation arcs (hereafter named HERA v1 and v2 lattices). Figure 5 shows the Twiss functions and momentum compaction functions of the two arcs. Although both lattices have the same geometric layout, they exhibit distinct optical behaviors through properly tuning quadrupole focusing strengths. HERA v1 is a 180-deg arc with large momentum compaction. Moreover, it is a second-order achromat and *globally* isochronous with a large dispersion modulation across the entire arc [see Figs. 5(a) and 5(c)]. By contrast, HERA v2 is also a 180-deg arc with however small momentum compaction. This arc is also a second-order achromat but is designed to be a *locally* isochronous lattice within superperiods. Such local isochronicity ensures that the bunch length be kept the same at phase homologous CSR emission sites [see Figs. 5(b) and 5(d)]. Notably, it is shown in Figs. 5(c) and 5(d) that the momentum compaction function $R_{56}(s)$ for HERA v2 is considerably smaller in amplitude compared with that for HERA v1 by at least 2 orders of magnitude due to local isochronicity.

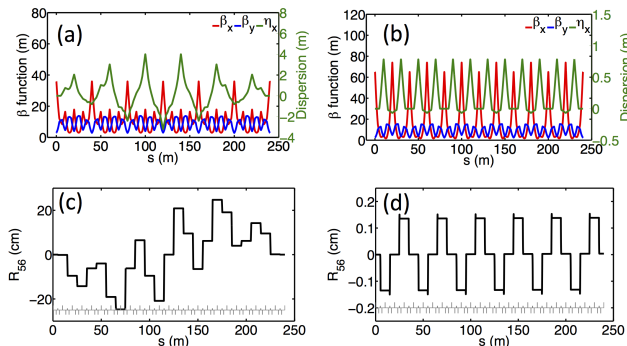


Figure 5: Twiss functions and $R_{56}(s)$ for HERA v1 (a,c) and v2 (b,d).

For both examples, the (peak) beam current is chosen to be 65 A, the transverse normalized emittances are assumed $0.3 \mu\text{m}$, and the uncorrelated energy spread is assumed 1.23×10^{-5} . These beam parameters are typical for next-generation light source facilities based on recirculation or ERL machines. Figure 6 shows the CSR-induced microbunching gain spectra for HERA v1 and v2 arcs, respectively. They were calculated with our developed semi-analytical Vlasov solver [26]. A dramatic difference of CSR gain between the two examples is clearly indicated. To validate the Vlasov results, we benchmark the two example lattices by using elegant [27], with which extensive convergence studies were performed [28]. Both our Vlasov solution and elegant tracking show excellent agreement in microbunching gain estimation.

05 Beam Dynamics and EM Fields

D05 Coherent and Incoherent Instabilities - Theory, Simulations, Code Developments

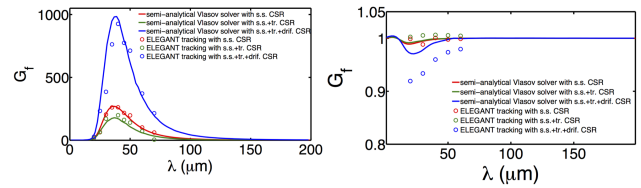


Figure 6: CSR microbunching gain spectrum for HERA v1 (left) and v2 (right). The dots are taken from particle tracking simulation by elegant. For HERA v1, the initial density modulation is set 0.05% for steady-state case; 0.06% for steady-state and entrance-transient case; 0.01-0.04% for all relevant CSR effects including entrance, exit transients and steady-state CSR. With larger gain, to keep the microbunching process remaining in the linear regime, it is required the initial modulation amplitude be smaller (see also comments in the context). For HERA v2, the initial modulation amplitude is set 0.8% and the same number of macroparticles as HERA v1 is used. For HERA v2, the apparent difference between Vlasov solutions and elegant tracking is actually small; note the vertical scale in small numerics.

Now let us examine our proposed conditions for the two example arcs. Figure 7 (a) and (b) compares Twiss α functions at dipole locations and betatron phase differences ψ_{21} between near-neighbor dipoles. As mentioned, moderate α function [Fig. 7(b)] is usually not a bad choice to produce small relative momentum compaction. The phase differences between near-neighbor dipoles for the two examples are illustrated in Fig. 7 (c) and (d), respectively. HERA v2 with ~ 0 or $\sim \pi$ phase difference between adjacent dipoles indeed satisfies our proposed condition that smaller relative momentum compaction can be achieved when $\psi_{21} \approx \pi$ (or its integer multiples). In contrast, HERA v1 with scattering from 0 to $\pi/2$ does not meet our proposed condition of phase difference. At dipoles, $\beta_x \leq 10$ m for the two examples are comparable (not shown here). It turns out that the maximal magnitude of $R_{56}^{s' \rightarrow s}$ for HERA v1 is four times larger than that of HERA v2. It is this difference in $R_{56}^{s' \rightarrow s}$ that makes the distinct CSR microbunching development.

To further evaluate the performance of the lattice designs, for each dipole pair as a two-dipole module, we vary the nominal values of Twiss functions in a range and see where the design value of the momentum compaction $R_{56}^{s' \rightarrow s}(\alpha_{x0}, \beta_{x0}, \psi_{21})$ locates in the parameter space $(\alpha, \beta, \psi_{21})$, where $\alpha \in (0.1\alpha_{x0}, 10\alpha_{x0})$, $\beta \in (0.1\beta_{x0}, 10\beta_{x0})$, and $\psi_{21} \in (0, 2\pi)$. Then we consider a pair to be dangerous once the nominal $R_{56}^{s1 \rightarrow s2}(\alpha_{x0}, \beta_{x0}, \psi_{21})$ is larger than 80% of maximum value in the parameter space $\max\{R_{56}^{s1 \rightarrow s2}(\alpha, \beta, \psi_{21})\}$. Having examined all possible pairs of the two-dipole modules for HERA v1, we found 27 pairs (among a total of 276 combinations) are indicated as *dangerous* pairs and 12 of them are from near-neighbor dipoles. For HERA v2, all the near-neighbor pairs are evaluated to be *safe*.

The parameters Λ and ξ can be used to scale the maximal gain for comparative lattices. It is found that ξ for HERA

Content from this work may be used under the terms of the CC BY 3.0 licence (© 2018). Any distribution of this work must maintain attribution to the author(s), title of the work, publisher, and DOI.

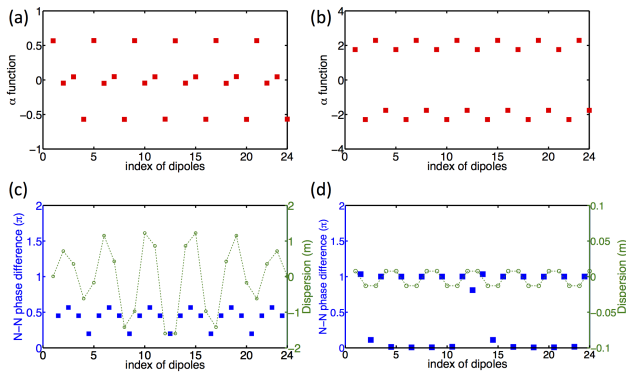


Figure 7: Twiss α functions at dipoles and betatron phase differences ψ_{21} (in unit of π) for HERA v1 (a,c) and v2 (b,d). The dashed lines in (c) and (d) only help visualize the dispersion within dipoles.

v1 is about 6.4 times larger than that of HERA v2 [25]. We see in Fig. 8 that indeed this multiplicative factor can reflect the scaling of bunch current for the maximal gains. This scaling can be used as a guideline of setting the order of magnitude of the maximal relative momentum compaction function $R_{56}^{s' \rightarrow s}$ (via \mathcal{K}) for specified design goals. Assume we have already known the performance of HERA v2 and had no a priori detailed study of CSR microbunching about HERA v1.

Now we want to estimate under what level of beam current can the beam be transported through HERA v1 with little CSR microbunching effect. Provided HERA v1 lattice is given, ξ can be determined and compared with that of HERA v2. We then expect that a circulating beam with peak current six times smaller than that of nominal one of HERA v2, i.e., ~ 10 A or six-times smaller Λ , should not be subject to CSR microbunching instability. This is immediately confirmed in the figure.

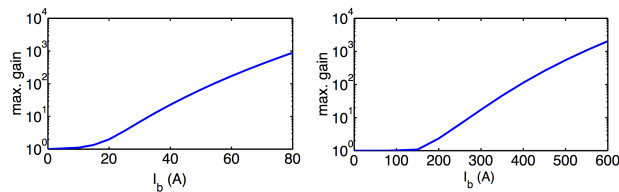


Figure 8: Dependence of maximal CSR gains of HERA v1 (left) and v2 (right) on initial (peak) bunch current.

As described, HERA v2 satisfies all requirements of CSR suppression, and is therefore expected to preserve the beam phase space qualities. For reference, the resultant CSR-induced emittance growths and microbunching gains for the two Examples are shown in Fig. 9, from which one can see the transverse beam emittance at the exit of the arc is well preserved in HERA v2 while features four times increase for 500 pC in HERA v1.

To end this section, it may deserve here to comment on the relation between the study in Ref. [24] and the present analysis to suppress CSR-induced MBI. Here we quantified

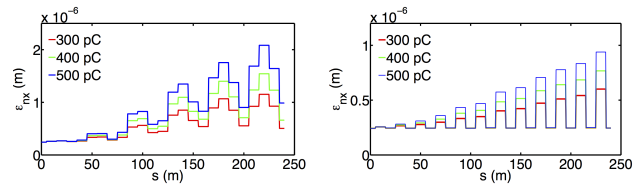


Figure 9: Evolution of the transverse normalized emittances for HERA v1 (left) and HERA v2 (right) lattices.

the lattice performance to CSR microbunching effect by the dimensionless parameter ξ . From the multistage CSR analysis [24], it can be seen that the final gain (up to M -th stage) $\left| \tilde{G}_f^{(M)} \right| \sim \sum_{m=0}^M [\Lambda \xi A \{L.D.; s, s'\}]^m$. For the presented examples, $\Delta L \approx 40$ m for HERA v1 and $\Delta L \approx 20$ m for HERA v2 arcs. Here the proposed conditions aim to make ξ as small as possible, lead to smallness of kernel function \mathcal{K} , and thus small microbunching gain in general. The two differences, however, should be highlighted here: (i) the quantity ξ does not take Landau damping into account. That is, the proposed conditions are sufficient and not exclusive, and (ii) the present analysis only accounts for $m = 1$ case from the viewpoint of multistage CSR analysis [24]. It should be straightforward that a first-iterative beamline design, as well as the first-stage CSR microbunching amplification, may start from the lowest order and later deal with higher order effects.

SUMMARY AND CONCLUSION

In this paper we have given an overview of various mitigation schemes of CSR-induced effects, including compensation of CSR-induced emittance growth in the transverse domain and suppression of microbunching instability in the longitudinal dimension. We proposed and verified the validity of sufficient conditions for effective suppression of CSR-induced microbunching gains in recirculation arcs. The conditions of preferring small β functions, avoiding vanishingly small α functions within dipoles, and of keeping $\psi_{21} \approx m\pi$, with m to be an integer, in consecutive two-dipole modules, aim for minimizing ξ (hence \mathcal{K}) through the relative momentum compaction function $R_{56}^{s' \rightarrow s}$ in a beamline design. Those conditions apply to both periodic and non-periodic magnetic lattices, from low to high energy regimes, and for constant as well as varying bunch length along a beamline [25].

In the most general case of non-achromatic and non-isochronous beamline, the constraint of betatron phase difference can be weakened (or values slightly deviated from $m\pi$ may be preferred [25]), depending on the specific lattice design. In that sense, extracting $R_{56}^{s' \rightarrow s}$ from Eq. (5) can be used to examine or optimize a beamline design when CSR microbunching becomes a concern.

Since the CSR-induced instability is intensity dependent, our proposed conditions can minimize the CSR-induced microbunching for any given electron bunch current. The set of comparative example lattices can prove useful for

beamline designs at difference energies or bunch currents through the scaling parameter. We have thus investigated the scaling of beam current for maximum CSR gains, and it can serve as a guideline of setting the maximal magnitude of the relative momentum compaction to be designed for similar purposes at different level of bunch currents or beam energies.

ACKNOWLEDGEMENTS

The author would like to take this opportunity to thank Dr. Juhao Wu (SLAC) for his support to the continuation of this work, Prof. Mark Pitt (Virginia Tech), and Drs. Rui Li, Steve Benson, Dave Douglas, and Chris Tennant (JLab) and Simone Di Mitri (FERMI) for their support, inputs, encouragement and stimulating discussions during the past few years.

REFERENCES

- [1] M. Borland, "Start-to-end jitter simulations of the Linac Coherent Light Source", in Proceedings of the 19th Particle Accelerator Conference, Chicago, IL, 2001 (IEEE, Piscataway, NJ, 2001), WPPH103.
- [2] S. Heifets, G. Stupakov, and S. Krinsky, "Coherent synchrotron radiation instability in a bunch compressor", *Phys. Rev. ST Accel. Beams* 5, 064401 (2002).
- [3] Z. Huang and K.-J. Kim, "Formulas for coherent synchrotron radiation microbunching in a bunch compressor chicane", *Phys. Rev. ST Accel. Beams* 5, 074401 (2002).
- [4] R. Hajima, "A first-order matrix approach to the analysis of electron beam emittance growth caused by coherent synchrotron radiation", *Japanese Journal of Applied Physics*, 42 (2003)
- [5] Y. Jing, Y. Hao, and V. N. Litvinenko, "Compensating effect of the coherent synchrotron radiation in bunch compressors", *Phys. Rev. ST Accel. Beams* 16, 060704 (2013)
- [6] D. Douglas *et al.*, "Control of coherent synchrotron radiation and microbunching effects during transport of high brightness electron beams", arXiv: 1403.2318v1 [physics.acc-ph]
- [7] D. Douglas *et al.*, "Control of synchrotron radiation effects during recirculation", IPAC15 (TUPMA038)
- [8] D. Douglas, "Suppression and enhancement of CSR-driven emittance degradation in the IR-FEL Driver", JLAB-TN-98-012, 1998
- [9] D. Douglas *et al.*, "Control of synchrotron radiation effects during recirculation with bunch compression", IPAC15 (TUPMA037)
- [10] S. Di Mitri, M. Cornacchia, and S. Spampinati, "Cancellation of Coherent Synchrotron Radiation Kicks with Optics Balance", *Phys. Rev. Lett.* 110, 014801 (2013)
- [11] Y. Jiao, X. Cui, X. Huang, and G. Xu, "Generic conditions for suppressing the coherent synchrotron radiation induced emittance growth in a two-dipole achromat", *Phys. Rev. ST Accel. Beams* 17, 060701 (2014)
- [12] S. Di Mitri and M. Cornacchia, "Transverse emittance-preserving arc compressor for high-brightness electron beam-based light sources and colliders", *EPL* 109, 62002 (2015)
- [13] S. Di Mitri, "CSR-induced emittance growth and related design strategies", *USPAS Lecture Note of Linear Accelerator Design for Free Electron Lasers* (2015)
- [14] C. Mitchell, J. Qiang, and P. Emma, "Longitudinal pulse shaping for the suppression of coherent synchrotron radiation-induced emittance growth", *Phys. Rev. ST Accel. Beams* 16, 060703 (2013)
- [15] P. Emma and R. Brinkmann, "Emittance dilution through coherent energy spread generation in bending systems", *Proceedings of Particle Accelerator Conference 1997*
- [16] M. Venturini, "CSR-induced emittance growth in achromats: Linear formalism revisited", *NIM A* 794 (2015), pp. 109-112
- [17] M. Venturini, "Design of a triple-bend isochronous achromat with minimum coherent-synchrotron-radiation-induced emittance growth", *Phys. Rev. Accel. Beams* 19, 064401 (2016)
- [18] Ya. S. Derbenev, J. Rossbach, E. L. Saldin, and V. D. Shiltsev, "Microbunch radiative tailhead interaction", *TESLA-FEL-Report 1995-05*
- [19] E. L. Saldin, E. A. Schneidmiller, and M. V. Yurkov, "Longitudinal space charge-driven microbunching instability in the TESLA Test Facility linac", *NIM A* 528 (2004), pp. 355-359
- [20] Z. Huang *et al.*, "Suppression of microbunching instability in the linac coherent light source", *Phys. Rev. ST Accel. Beams* 7 074401 (2004)
- [21] S. Di Mitri and S. Spampinati, "Microbunching instability suppression via electron-magnetic-phase mixing", *Phys. Rev. Lett.* 112, 134802 (2014)
- [22] C. Behrens, Z. Huang, and D. Xiang, "Reversible electron beam heating for suppression of microbunching instabilities at free-electron lasers", *Phys. Rev. ST Accel. Beams* 15, 022802 (2012)
- [23] J. Qiang, C. Mitchell, and M. Venturini, "Suppression of microbunching instability using bending magnets in free-electron-laser linacs", *Phys. Rev. Lett.* 111, 054801 (2013)
- [24] C.-Y. Tsai, D. Douglas, R. Li, and C. Tennant, "Multistage CSR microbunching gain development in transport or recirculation arcs", *FEL15 (MOP087)*
- [25] C.-Y. Tsai, S. Di Mitri, D. Douglas, R. Li, and C. Tennant, "Conditions for coherent-synchrotron-radiation-induced microbunching suppression in multibend beam transport or recirculation arcs", *Phys. Rev. Accel. Beams* 20, 024401 (2017)
- [26] C.-Y. Tsai, D. Douglas, R. Li, and C. Tennant, "Linear microbunching analysis for recirculation machines", *Phys. Rev. Accel. Beams* 19, 114401 (2016)
- [27] M. Borland, "elegant: A Flexible SDDS-Compliant Code for Accelerator Simulation", *APS Light Source Note LS-287* (2000)
- [28] C.-Y. Tsai and R. Li, "Simulation of coherent synchrotron radiation induced microbunching gain using elegant", *JLAB-TN-14-016*